A Novel Signal Processing Scheme for Static Person Localization Using M-Sequence UWB Radars

Dušan Kocur, Tamás Porteleky, Mária Švecová, Michal Švingál, and Jana Fortes

***Abstract*—Developments in sensing technology have shown that UWB radars are becoming increasingly valuable sensing devices that can be used for monitoring of humans in military/police and civilian areas. It is known that the applicability of particular methods of human localization depends on the character of persons' motion. With respect to this finding, the researchers' attention has been aimed at two fundamental directions. While the former is focused on the localization of moving persons (MP), the latter approach is intended to localize static persons (SP). Then, a proper fusion of the methods developed for MP and SP localization allows monitoring of persons moving with an unknown time-variable character of motion (MP-SP). The analyses of the currently known methods of MP and SP localization in terms of their use for MP-SP localization have shown that while MP localization methods are in principle well developed, SP localization methods are not sufficiently adapted for their use in MP-SP monitoring. Motivated by these findings, we would like to introduce a new radar signal processing procedure for SP localization (SPL) that could be an efficient component of algorithms to be applied for MP-SP monitoring. The novel features of the proposed SPL consist especially in a new approach to SP detection and inclusion of SP tracking in SPL. Moreover, SPL is characterized by relatively low computational complexity and is, therefore, suitable for real-time implementation. Experimental results have shown that SPL introduced in this paper provides very good performance for multiple person localization for line-of-sight and through-the-wall scenarios.**

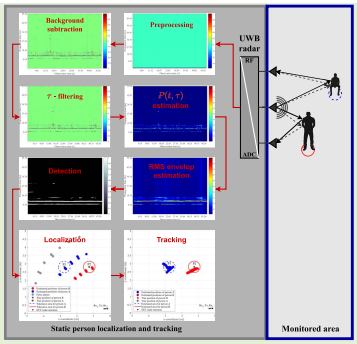

***Index Terms*— Breathing, detection, localization, signal processing, static person, tracking, ultra-wideband (UWB) radar.**

I. Introduction

PEOPLE detection, localization, and tracking belong among the oldest applications of UWB radars [1]. In this field, the attention of the researchers is split into two fundamental topics. The former is localization of moving persons (MP) [2], i.e., persons moving within a monitored area in such a way that their coordinates are changing. The latter is localization of static persons (SP) [3], i.e., persons situated, but not moving within the monitored area. The respiration motions are usually the only visible form of SP movement. A proper fusion of the methods developed for MP and SP detection and localization allows monitoring of persons moving with an unknown time-variable character of motion (MP-SP) [4]. Such functionality is usually requested by any localization system. A survey of the methods of MP localization presented e.g., in [4] and [5] have shown that, with respect to MP-SP monitoring, the developed approaches to MP localization can be considered well handled. However, the state-of-the-art in the field of SP localization has indicated thatcurrently available methods have not been sufficiently adapted for their exploitation for MP-SP monitoring. Their shortcomings in terms of this application will be summarized in the next paragraphs. Motivated by these findings, we would like to introduce in this paper a new radar signal processing procedure for SP detection and localization (SPL) that could be an efficient component of algorithms to be applied for MP-SP monitoring by multistatic M-sequence UWB radars [6].

Following the outlined aim, our paper is organized as follows. In the next section, the analyses of the state-of-the-art in the field of SP localization will be presented. As a result of

Manuscript received June 20, 2021; accepted June 27, 2021. Date of publication June 30, 2021; date of current version September 15, 2021. This work was supported in part by Slovak Research and Development Agency under Contract APVV-18-0373 and in part by Scientific Grant Agency (VEGA) under Contract 1/0584/20. The associate editor coordinating the review of this article and approving it for publication was Prof. Piotr J. Samczynski. *(Corresponding author: Mária Švecová.)*

Dušan Kocur and Jana Fortes are with the Department of Electronics and Multimedia Communications, Technical University of Košice, 042 00 Košice, Slovakia (e-mail: dusan.kocur@tuke.sk; jana.fortes@tuke.sk).

Tamás Porteleky and Michal Švingál are with the K-Mlab Organizational Unit of Ilmsens GmbH, 040 01 Košice, Slovakia (e-mail: tamas.porteleky@ilmsens.com; michal.svingal@ilmsens.com).

Mária Švecová is with the Department of Mathematics and Theoretical Informatics, Technical University of Košice, 042 00 Košice, Slovakia (e-mail: maria.svecova@tuke.sk).

Digital Object Identifier 10.1109/JSEN.2021.3093658

this section, a specification of requested properties of SPL to be exploited for MP-SP monitoring will be given in Section III. The core of the paper (Section IV) is focused on a new original SPL satisfying the requirements summarized in Section III. Some experimental results illustrating the performance of the proposed approach of SP localization will be shown in Section V. In the last section, some concluding remarks will be summarized.

II. Related Work

A. Raw Radar Signals

In the case of people monitoring by using an M-sequence UWB radar, raw radar signals (or radar scans) are represented by a set of impulse responses of the environment, through which the electromagnetic waves emitted by the radar are propagated from transmitting radar antenna (Tx) to receiving radar antenna (Rx). The radar scans thus defined can be modeled by the expression

$$h(t,\tau) = f(s(t,\tau), n(t,\tau), c(t,\tau), i(t,\tau), j(t,\tau)), \quad (1)$$

where t, τ, $s(t,\tau)$, $n(t,\tau)$, $c(t,\tau)$, $i(t,\tau)$ and $j(t,\tau)$ denote the propagation time, observation time, radar echos, noise generated by radar circuitry, clutter, interference, and jamming, respectively [4]. The operator $f(\cdot)$ represents the input-output model of an analog front–end of a radar receiving channel. If the radar receiver is operating in a linear region of its analog front–end, and if there is no interference and jamming, then (1) can be expressed in the following simplified form

$$h(t,\tau) = s(t,\tau) + n(t,\tau) + c(t,\tau). \quad (2)$$

In general, the radar echo $s(t,\tau)$ is a signal due to the portion of the energy of those transmitted electromagnetic waves which have been reflected by a target and which have been subsequently received by a radar receiver. In the case of UWB radars applied for person monitoring, the backscatters can be due to electromagnetic wave multipath propagation very complex. It has been shown in [7]–[9] that the Saleh-Valenzuela model could be used to model the impulse response of the UWB channel. According to this model, backscatters propagating along several individual paths come to Rx in the form of clusters. Such a cluster can be defined as a set of multipath components with similar arrival times, and in the case of UWB signals transmission, with exponentially decaying amplitudes as well. The first detected backscatter situated in the first received cluster is usually used to estimate the time-of-arrival (TOA) of the target. In the next, this component of the backscatters will be referred to as the main component of the radar echo. On the other hand, additional backscatters located in the second and other clusters can cause the formation of ghosts [9].

As follows from microwave circuit theory, crucial parts of the noise $n(t,\tau)$ are generated by Rx and an analog front-end of the radar receiver. Considering these facts, we can assume that $n(t,\tau)$ is a zero-mean stationary additive white Gaussian noise (AWGN) [6].

The clutter $c(t,\tau)$ is given by backscatters from objects situated in the monitored area that are not the desired targets, and signals obtained as the results of antenna coupling and impedance mismatch of the RF circuits of the radar device.

Let us assume that sampling frequency of $h(t,\tau)$ along the axes t and τ will be denoted f_t and f_τ, respectively. Then, the radar range resolution is $\Delta d = c/f_t$, where $c = 3 \times 10^8$ ms^{-1} is the electromagnetic wave propagation velocity in the air. Another important parameter of the radar is its measurement rate r expressing the total number of radar scans taken per second. In general $r \neq f_\tau$. A set of M consecutive radar scans $H_M(t,\tau) = \{h(t, texttau - k), k = 0, 1, 2, \ldots, M-1\}$ is usually referred to as a radargram defined for an observation time interval $L_M^\tau = M/f_\tau$. Let the length of the impulse response sensed by the radar be $L_N^t = N/f_t$, where N is the total number of samples of the impulse response. Then $H_M(t,\tau)$ is a matrix of $N \times M$ type. A sample of the radargram $H_M(t_j, \tau_k)$ represents a sum of electromagnetic wave reflections from all objects with the same bistatic range

$$d(t_j, \tau_k) = ct_j \quad (3)$$

sensed at the observation time instant τ_k. Then, the j-th row of radargram

$$H_M(t_j, \tau) = \{h(t_j, \tau - k), k = 0, 1, 2, \ldots, M-1\} \quad (4)$$

represents a sequence of the sums of electromagnetic wave reflections from all objects with the constant bistatic range expressed by (3) obtained by successive measurements taken in the observation time interval L_M^τ.

B. Basic Principles of SP Detection

Basic issues of SP detection have been studied in many publications (e.g., [10]–[14]). The solutions developed in these papers assume that the respiration motions are usually the only detectable form of SP movement. Then, the starting point of the proposed methods of SP detection is the precondition that a human being's breathing can be considered a periodical process with a fundamental harmonic frequency $f_B \in F_B = \langle 0.16 \text{ Hz}, 1 \text{ Hz} \rangle$ [15]. The motions of the human respiratory tract during inhalation and exhalation directly affect the movement of other parts of the human body such as the thorax, abdomen, back, etc. Then the movement of these parts of the human body can also be considered a periodic process with the same fundamental harmonic frequency $f_B \in F_B$. The amplitudes of these motions are relatively small and depend on the specific part of the human body. For example, the peak-to-peak value of chest movement due to respiration in adults is about $0.4 - 1.2$ cm [11]. Now that we consider that the range resolution of the UWB radar is about $1 - 3$ cm, then the backscatters due to the same part of the SP body should still be located at the same bistatic range for all moments of observation time. These signals should be located in the radargram row and should contain components of harmonical signals with frequencies $f_B \in F_B$.

Then for SP detection, the following basic rule can be applied. Firstly, the total power of $H_M(t_j, \tau)$ per L_M^τ in the

frequency band F_B denoted as $P\left(t_j, \tau\right)$ is estimated. Then if

$$P\left(t_j, \tau\right) \geq \gamma\left(\tau\right), \tag{5}$$

where $\gamma\left(\tau\right)$ is a threshold, SP is detected in the j-th row of the radargram. The TOA and the bistatic range of thus detected SP are t_j and $d\left(t_j, \tau\right)$, respectively. The mentioned rule is very free (how to estimate $P\left(t_j, \tau\right)$, how to choose $\gamma\left(\tau\right)$). And hence, its practical implementation leads to many variants of SP detection methods.

It is known from the detection theory, that the higher the radar echo-to-noise and clutter ratio ($ENCR$), the higher the probability of target detection (P_D) as well. Because the $ENCR$ for SP detection is usually very low, it should be improved before the implementation of any methods of SP detection. As a result, the process of the SP detection is usually decomposed at least into three stages, which include noise and clutter suppression, an estimation of $P\left(t_j, \tau\right)$, and finally the detection itself [4].

C. SP Detection and Ranging: State-of-the-Art

An interesting and still actual approach for SP detection introduced in [13] and [16] is divided into the following stages: decreasing of total level of AWGN (range filtering, slow-time frequency domain windowing), stationary clutter removal (range-profile, mean, and linear trend subtraction), nonstationary clutter suppression (a singular value decomposition (SVD) method), the power spectrum estimation using, e.g., fast Fourier transform (FFT), and finally threshold-based decision and range-estimation stage. The proposed approach has been successfully demonstrated for the detection of a single person located under rubble.

A bit different approach for SP detection has been proposed in [11]. In this contribution, high-pass filtering in observation time and SVD have been recommended for static and non-stationary clutter suppression, respectively. The power spectrum is estimated using an auto-correlation of radargram rows across the propagation-time window centered at the expected TOA corresponding to a target. As an alternative approach to power-spectrum estimation, the Welch periodogram is mentioned in [11]. The obtained results have shown that the discussed method has been successfully used for complex scenarios such as ranging of a single SP situated under heavy rubble or localization of SP through the three floors of the building.

In [17], a sensor network of bistatic UWB radars for multiple person localization has been introduced. The employed signal processing scheme consists of $ENCR$ improvement phase (moving target indicator, passband filtering along the τ-axis), detection (ranges and breath frequencies of potential targets are detected from cross-spectral density calculated from preprocessed signals), an initial screening focused on a reduction of some potential targets and target localization (a maximum likelihood observation-target association technique employed for ranges and breathing frequencies association and human target localization). The bistatic UWB radar network according to [17] has been able to provide not only good localization of one to three SPs for a simple line-of-sight (LOS) scenario but also to estimate persons' breathing rates.

The method referred to as WP-STAPELOC has been introduced in [3]. This approach for multiple SPs localization consists of the set of five signal processing phases such as background subtraction (exponential averaging method), target-echo enhancement (range filtering, low-pass filtering along τ-axis), target detection, TOA estimation and TOA association (trace connection method), wall effect compensation (trace correction of the first or second kind), and target localization (direct computation method). For SP detection, a two-stage detector consisting of a power spectrum estimator (Welch periodogram method), order statistics constant false alarm detector (OS-CFAR), and a simple threshold detector have been employed. The performance properties of the WP-STAPELOC method have been demonstrated by a successful high-accuracy through-the-wall (TW) localization of three SPs.

An improvement of the WP-STAPELOC method has been introduced in [18] and [19]. In these papers, the WP-STAPELOC method was supplemented by the target tracking phase implemented by a multiple target tracking system (MTT). In this case, SP tracking allows handling the situation when the number of targets is changing. The experimental results presented in [18] and [19] have shown that the modified version of WP-STAPELOC has been able to detect, localize and track multiple SP, for LOS and TW scenarios, including scenarios with changing number of SPs. In both papers, a real-time operating implementation of the modified WP-STAPELOC method has been presented as well.

Detection of the presence of individuals including SP has been studied in [20]. This work is interesting mainly in that it has dealt with the detection of SP lying down in a heavy clutter environment. For the clutter reduction, background subtraction methods referred to as the reference method or running average filtering, and SVD have been considered. To detect SP, a two-stage detection process employing two cell-averaging CFAR detectors has been proposed. This processing scheme of signals measured by impulse UWB radar has allowed detecting not only the presence of SP lying down but also to monitor the presence of SPs if their number is changing.

The above-described approaches to SP detection and ranging have a lot of modifications in the field of methods of noise and clutter suppression, $P\left(t_j, \tau\right)$ estimation, and finally the detection itself. Therefore, a shortlist of some important alternative approaches to solutions to these issues is given in the next paragraphs.

The analyses of other contributions focused on selected issues of SP detection (e.g., [11], [21]–[23], etc.) have shown that not only conventional, but also iterative SVD method [24], correlation analyses of radargram rows [11], [17], Curvelet transformation [25], and CLEAN algorithm [26] can be used for the $ENCR$ improvement. Besides traditional methods of power spectrum estimation, the utilization of time-frequency transformation has been proposed for the radargram row power spectrum estimation. The methods such as Hilbert-Huang transformation (e.g., [23], [25], [27]–[29]), S-transformation [30], wavelet transformation [31], and wavelet entropy [32] can be rated among them.

There are also several alternative approaches to SP detection compared to the relationship based approach (5). In these cases, instead of $P\left(t_j, \tau\right)$, other quantities having relation to $P\left(t_j, \tau\right)$ are employed. Such approaches have been mentioned e.g., in [33]–[38], where instead of $P\left(t_j, \tau\right)$, the 8th order cumulants [33]–[35], [37], or so-called harmonograms [36], [38] have been used. An experimental comparison of the performance of SP detectors based on the application of variance, standard deviation, kurtosis, and skewness presented in [37] has indicated that application of the variance provides probably the best results for SP detection and ranging.

The analysis of the contributions referred to in this section has shown that these works do not practically consider the problem of the computational complexity of the signal processing methods that they employ. Regarding this issue, it is useful to distinguish between single scan signal processing methods (SS-M) and block scan signal processing methods (BS-M). In the case of SS-M, a single current radar scan is used as input for the method under consideration. The method of exponential averaging frequently applied for clutter suppression is a good example of SS-M [39]. On the other hand, in the case of BS-M, a block of scans is used as input for the method under consideration. The SVD [39] or FFT [3] are the typical representatives of BS-M. As the BS-Ms are based on matrix computation of usually large matrices, they belong among methods that are characteristic by high-computational complexity. Then, if possible, it is advisable to avoid the use of BS-Ms in the SP detection.

Another weakness of current articles focused on SP detection and localization is that they usually do not deal with the issue of the value of sampling frequency along the τ-axes (f_τ) and the rate (frequency) of generating the target coordinate estimate $\left(f_{\tau_g}\right)$. Many contributions present the results of SP localization as the results of processing just one radargram (e.g. [3]). On the other hand, there are only a few articles (e.g. [19]) that report the results of SP localization generated with some frequency f_{τ_g}. From a practical point of view, the results of SP localization should be generated with frequency $f_{\tau_g} = f_\tau$. This requirement is particularly important if the considered SP localization method should be used as part of a signal processing scheme for MP-SP monitoring.

Taking into account the knowledge summarized in this section, we will introduce in the next sections a novel computationally efficient, and robust signal processing scheme for SP localization.

III. Problem Statement

A novel SPL with the following properties should be developed in this paper:

- SPL should allow localization of SP in the $x - y$ plane for $y \geq 0$ using a multistatic M-sequence UWB radar operating with 1 Tx and 2 Rx, whose coordinates are

$$Tx = (0, 0), \quad Rx_1 = (x_1, y_1) = (d, 0), \\ d > 0, \quad Rx_2 = (x_2, y_2) = (-d, 0). \tag{6}$$

- SPL should allow localization and tracking of multiple human targets including the scenarios with a time-variable number of SPs.
- SPL should be usable as a part of signal processing schemes for MP-SP monitoring.
- SPL should be suitable for real-time implementation (i.e. the SPL computational complexity and sampling frequency f_τ should be as low as possible).
- SPL should be suitable for SP localization for LOS indoor as well as TW scenarios.
- SPL should support SP localization using baseband and passband operating UWB radars, including UWB radars satisfying the standard of the European Electronic Communications Committee [40].

IV. Signal Processing Scheme for SP Localization

Based on the properties of raw radar data and the state-of-the-art related to this issue, we propose to use for SP localization the SPL consisting of seven basic phases of signal processing which include raw radar data preprocessing, background subtraction, target detection, TOA estimation and TOA association, wall effect compensation, target localization, and target tracking. In the following sections, we will explain the importance of the particular phases and introduce the appropriate signal processing methods that can be used in these phases.

A. Raw Radar Data Preprocessing

This phase of SPL aims to set up the sampling frequency f_τ as well as to reduce the level of $n\left(t, \tau\right)$, and thus improve $ENCR$.

As we have shown above, the respiration rate of a human being is $f_B \in F_B = \langle 0.16\ \text{Hz}, 1\ \text{Hz}\rangle$. In the case of SP localization, the respiration motion of persons is the only form of movement that could be detected by the radar. Then, according to the Nyquist–Shannon sampling theorem, the sampling frequency of raw radar signals along the τ-axis should satisfy the condition

$$f_\tau \geq 2 \max F_B = 2\ \text{Hz} \tag{7}$$

However, as a rule, the sampling frequencies are usually chosen higher than the minimum sampling frequency given by the sampling theorem. Following this rule, we propose to sample the raw radar data along the τ-axis with the frequency $f_\tau \approx 4$ Hz. The suitability of such a choice of f_τ was confirmed by many experimental measurements focused on SP monitoring, which we have performed with UWB radars.

For a reduction of the level of AWGN contained in the raw radar signals, we propose to employ synchronous averaging of original radar scans and range filtering (filtering of radar scans along the t-axis) [6].

In the case of SP monitoring, the target motions are slow compared to the radar measurement rate. This step opens up the opportunity to apply synchronous averaging by which the noise performance of the measurement will be considerably improved and additionally the data throughout will be reduced [6]. Following this basic idea, synchronous averaging can be applied if the rate of measurement r is higher than that of the sampling frequency f_τ, i.e., if

$$r > f_\tau. \tag{8}$$

A typical rate of measurement of M-sequence UWB radars could take on values from the interval 100-1000 impulse responses/s. And hence, condition (8) is usually very well met.

Let us assume that $h_r(t,\tau)$ are raw radar scans measured by a radar with measurement rate r, and $h(t,\tau)$ are resampled original scans (so-called resampled scans) obtained by synchronous averaging of L original scans, and hence sampled with the frequency $f_\tau = 1/\tau_s = r/L$. In the case of SP localization, we will assume that for a given r, L is chosen in such a way that $f_\tau \approx 4$ Hz. Then, the synchronous averaging of L original scans can be described by the expression

$$\begin{aligned} h\left(t,\tau_j\right) &= h\left(t, j\tau_s\right) = h\left(t, j/f_\tau\right) = h\left(t, j\left(L/r\right)\right) \\ &= \frac{1}{L}\sum_{l=0}^{L-1} h_r\left(t, (j+1)\left(\text{L-l}\right)/r\right) \\ &\quad \text{for } j = 0, 1, 2, \cdots, N-1. \end{aligned} \tag{9}$$

Synchronous averaging according to (9) represents a simplified form of a multichannel signal downsampling that does not use any anti-aliasing filters. Comparison of the experimental results from many testing scenarios showed that the synchronous averaging, implemented as the combination of hardware and software averaging, produces acceptable outputs, i.e. the effect of aliasing is negligible in this case. On the other hand, we have gained a positive feature, which is reduced computing complexity. Because respiration movements are much slower compared to r, and $n(t,\tau) \sim N\left(0, \sigma_n^2\right)$, synchronous averaging allows for reducing the level of noise components of $h(t,\tau)$, and thus to increase $ENCR$ [6].

If the fluctuations in the noise signal behave more abruptly than the variations in the target echo, the noise can be reduced by limiting the bandwidth. Then, $ENCR$ could be improved by range filtering of the particular impulse responses obtained as the results of synchronous averaging of original raw radar scans [6]. The range filtering of $h(t,\tau_k)$ along the t-axis can be formally expressed as

$$h_{Ft}(t,\tau_k) = F_t\left[h(t,\tau_k)\right], \tag{10}$$

where $F_t[\cdot]$ is an operator applied to the model filtering process. In the case of SP monitoring, band-pass filters are usually used for range filtering. The filter parameters, such as cut-off frequencies, bandwidth, attenuation in the stop band, etc., depend on the radar operation parameters, antennas and raw radar signal properties. The application of filters can result in a signal delay due to non-zero group delay of the filter. If such a delay is not acceptable, then the application of so-called zero-delay range filters is recommended [41]. Based on our practical experiences, we use the zero-phase elliptical filter of the 8th order only in the case when the radar signals are measured by a radar network. Then such a range filter suppresses the noise due to partial interference between radars working at the same time and in the same frequency band [6].

B. Background Subtraction

The second phase of SPL is focused on clutter suppression using background subtraction methods. By the term background, we understand stationary and correlated clutter, such as antenna coupling, impedance mismatch response, and ambient static clutter. If $\hat{b}(t,\tau)$ expresses an estimate of the background $b(t,\tau)$, then the background subtraction is given by the expression:

$$h_b(t,\tau_k) = h_{Ft}(t,\tau_k) - \hat{b}(t,\tau_k), \tag{11}$$

where $h_b(t,\tau_k)$ is the impulse response with a subtracted background. As follows from (11), the crucial issue of the background subtraction methods is the $b(t,\tau)$ estimation itself. The methods of the $b(t,\tau)$ estimation are based on the assumption that while the target echo can be considered a non-stationary component of $h_{Ft}(t,\tau)$, the background $b(t,\tau)$ is represented by stationary components of $h_{Ft}(t,\tau)$. Based on this assumption, a number of background estimation methods have been developed [42]. Because of good performance, high robustness, and low computational complexity, we propose to employ for the background estimation the method of exponential averaging [39]. According to this method, the background estimation $\hat{b}(t,\tau_k)$ is obtained by

$$\hat{b}(t,\tau_k) = \alpha\hat{b}(t,\tau_{k-1}) + (\alpha-1)\,h_{Ft}(t,\tau_k), \tag{12}$$

where $0 < \alpha < 1$ is a constant weighting factor setting the length of background estimator memory.

C. Target Detection

Detection methods analyze the impulse response with the subtracted background $h_b(t,\tau_k)$ and decide whether target backscatters are present or absent in the analyzed $h_b(t,\tau_k)$. For the SP detection, we propose to use the novel detection scheme shown in Fig. 1. Following this figure, we can see that firstly, the total power of the j-th rows of the radargram in the frequency band $F_B = \langle 0.16\,\text{Hz}, 1\,\text{Hz}\rangle$ denoted as $P\left(t_j,\tau_k\right)$ is estimated for $j = 0, 1, 2, \cdots, N-1$. To reduce the quantity of potential false alarms, root-mean-square (RMS) envelope of $P(t,\tau_k)$ denoted as $e_{RMS}(t,\tau_k)$ is computed. And then, the target detection itself is implemented using a two-stage detector where $e_{RMS}(t,\tau_k)$ are used as its primary testing statistics. In the next, we will describe the proposed SP detector in details.

As can be observed from Fig. 1, the $P\left(t_j,\tau\right)$ estimator consists of a τ-filter, an estimator of the instantaneous power of the signal, and an integrator. The τ-filter is used to limit the spectrum of the particular rows of the radargram with subtracted background $h_b\left(t_j,\tau\right)$ approximately to the frequency band F_B. The τ-filtering of $h_b\left(t_j,\tau\right)$ along the τ-axis can be expressed as

$$h_{F\tau}\left(t_j,\tau\right) = F\left[h_b\left(t_j,\tau\right)\right]. \tag{13}$$

As the τ-filter, we propose to use a low-pass IIR filter with the cut-off frequency of the pass-band $f_{F\tau} \approx 1$ Hz. Then a pass-band $F_{F\tau} = \langle 0\,\text{Hz}, 1\,\text{Hz}\rangle$ of the τ-filter can be considered as an acceptable approximation of the frequency band $F_B = \langle 0.16\,\text{Hz}, 1\,\text{Hz}\rangle$. We found out by experiments that as the τ-filter, a low-pass elliptic IIR filter of the 8th order can be applied with an advantage. Such selection of the τ-filter keeps the total computational complexity of τ-filtering at an acceptable level.

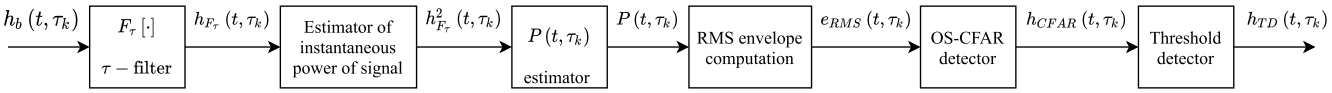

Fig. 1. SP detector applied to the k^{th} impulse response.

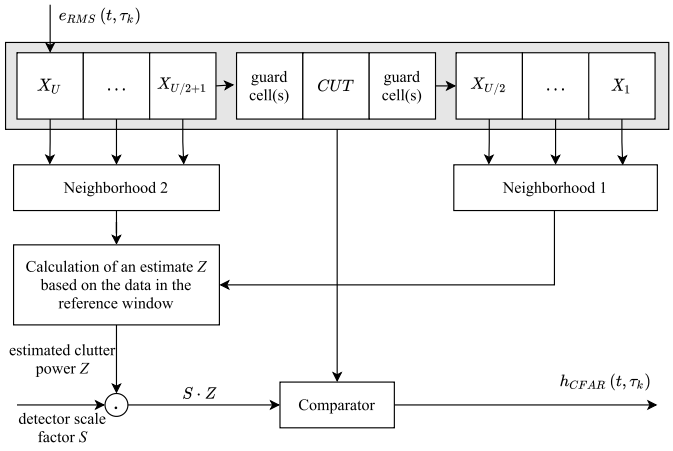

Fig. 2. OS-CFAR.

From what has been stated above is clear that $P\left(t_j,\tau_k\right)$ can be obtained as the estimation of the power of signal $h_{F\tau}\left(t_j,\tau_k\right)$ using the expression

$$P\left(t_j,\tau_k\right)=\beta P\left(t_j,\tau_{k-1}\right)+(\beta-1)\,h^2_{F\tau}\left(t_j,\tau_k\right) \quad \text{for } 0<\beta<1, \tag{14}$$

where $h^2_{F\tau}\left(t_j,\tau_k\right)$ has been obtained as the output of the estimator of the instantaneous power of $h_{F\tau}\left(t_j,\tau_k\right)$.

If we consider (5), $P\left(t,\tau_k\right)$ could be employed as the primary testing statistics of OS-CFAR. Our experimental analysis of $P\left(t,\tau_k\right)$ has shown that it provides SP detection, but at the same time, its usage produces a large number of false alarms. These false alarms are caused by residual noise and clutter fluctuation. To reduce these fluctuations and hence the number of false alarms as well, we propose to use instead of $P\left(t,\tau_k\right)$ its RMS envelope $e_{RMS}\left(t,\tau_k\right)$. Its utilization makes the process of SP detection more robust in comparison with simple lowering of the false alarms by setting the OS-CFAR detector parameters. The RMS envelope of the $P\left(t,\tau_k\right)$ can be calculated using a sliding window with the length W according to the following expression:

$$e_{RMS}\left(t_j,\tau_k\right)=\sqrt{\frac{1}{W}\sum_{l=0}^{W-1}P^2\left(t_{j-l},\tau_k\right)}. \tag{15}$$

The second part of SP detector shown in Fig. 1 is formed by a two-stage detector containing OS-CFAR and a simple threshold detector (TD). A basic block scheme of implemented OS-CFAR is shown in Fig. 2 (according to [43]–[45]). In comparison with a classic OS-CFAR approach, some guard cells are introduced to reduce self-interferences in a real target echo situation [45]. Following Fig. 2 and [44], the operation of the OS-CFAR can be described as follows.

The samples $e_{RMS}\left(t,\tau_k\right)$ are fed to a shift register of the OS-CFAR consisting of memory cells denoted as X_u. The key element of the shift register is referred to as the cell under test (CUT). The task of OS-CFAR is to decide if a sample located in CUT contains or does not contain a component due to the target backscatter. To make this decision, the data taken from the shift register cells X_u (reference window) are first rank-ordered according to increasing magnitude. The sequence thus achieved is called an ordered statistic

$$X_{(1)}\left(\tau_k\right)\le X_{(2)}\left(\tau_k\right)\le\cdots\le X_{(U)}\left(\tau_k\right), \tag{16}$$

where $X_{(1)}\left(\tau_k\right)$ denotes the minimum and $X_{(U)}\left(\tau_k\right)$ the maximum value. The central idea of an OS-CFAR procedure is to select one certain value $X_{(\upsilon)}\left(\tau_k\right)$, $\upsilon\in\{1,2,\cdots,U\}$ from (16) and use it as an estimate $Z\left(\tau_k\right)$ for the average clutter power observed in the reference window

$$Z\left(\tau_k\right)=X_{(\upsilon)}\left(\tau_k\right). \tag{17}$$

Then, the OS-CFAR threshold is

$$\gamma_{CFAR}\left(\tau_k\right)=Z\left(\tau_k\right)S, \tag{18}$$

where the scaling factor S depends on the OS-CFAR parameter U, the requested value of false alarm probability P_{FA}, and the probability density function of the clutter. In our application, we approximate the clutter probability density function by the exponential distribution and compute the scaling factor S according to the formulas described in [43]. The utilization of the RMS envelope allows us to set a constant value of false alarm probability ($P_{FA}=0.05$) for varied scenarios of SPL. Taken into account (17) and (18), the OS-CFAR output can be expressed as

$$h_{CFAR}\left(t_j,\tau_k\right)=\begin{cases}1 & \text{if } CUT\ge\gamma_{CFAR}\left(\tau_k\right)\\ 0 & \text{if } CUT<\gamma_{CFAR}\left(\tau_k\right),\end{cases} \tag{19}$$

where the value "1" ("0") indicates that a target reflection has been (has not been) detected in CUT.

It is well known that besides OS-CFAR, there are many variants of CFAR detector (e.g., [46]). Therefore, we have tested and compared the performance of several kinds of CFARs for the case of their employment in the detection stage of the SPL. The obtained results have shown the superior performance of OS-CFAR in combination with guard cells compared to other tested CFARs. For this reason, the described OS-CFAR was chosen for our SPL concept.

In the case of SP, the radar range resolution is much finer than the size of the person. Then, a human target has to be considered a distributed target. It means that several backscatters due to the same target can be detected. In order to avoid multiple detections of the same person, the second detection stage represented by TD is employed by the detection scheme

according to Fig. 1. The TD input $h_{TD}^{in}(t_j, \tau_k)$ is formed by the sequential summation of $h_{CFAR}(t_j, \tau_k)$ over the interval with the length V, where V represents approximately the maximum number samples of $h_{CFAR}(t_j, \tau_k) = 1$ that could be received from the same target. Then TD input is expressed as

$$h_{TD}^{in}(t_j, \tau_k) = \sum_{l=1}^{V} h_{CFAR}(t_{j-V+l}, \tau_k), \tag{20}$$

while the TD output is given by

$$h_{TD}(t_j, \tau_k) = \begin{cases} 1 & \text{if } h_{TD}^{in}(t_j, \tau_k) \geq \gamma_{HD} \\ 0 & \text{if } h_{TD}^{in}(t_j, \tau_k) < \gamma_{HD}, \end{cases} \tag{21}$$

where γ_{HD} is a constant integer expressing a TD threshold. It should fulfil the condition:

$$0 < \gamma_{HD} < V. \tag{22}$$

Similar to the OS-CFAR, $h_{TD}(t_j, \tau_k) = 1$ ($h_{TD}(t_j, \tau_k) = 0$) indicates that an SP has been (has not been) detected in $h_b(t, \tau_k)$ for $t = t_j$.

D. TOA Estimation and TOA Association

This phase of the SPL aims to process the output of the detection phase to estimate TOA of detected targets, to suppress some false alarms, and finally to associate TOAs estimated by Rx_1 and Rx_2 corresponding to the same target. For the solution of these tasks, we propose to use the trace connection method introduced in [47].

There are a few basic assumptions that allowed development of the trace connection method. The first assumption consists in an approximation of a human distributed target by a point target. Then, the only one TOA for one receiving channel is associated with a single SP. As we mentioned above, due to multipath electromagnetic wave propagation, target backscatters propagating along several individual paths come to Rx_i in the form of clusters where each cluster usually contains several target backscatters. Therefore, another assumption employed by the trace connection method is that the first detected and confirmed target backscatter in the first received cluster is used to estimate the target TOA. As it is shown in [47] during such TD output processing focused on detection and confirmation of the mentioned first target backscatter, a lot of false alarms are suppressed as well.

Then, as the results of this phase, two sets of TOAs are obtained for the observation time instant τ_k

$$TOA_{Rx_1}(\tau_k) = \left\{TOA_{Rx_1}^1, TOA_{Rx_1}^2, \cdots TOA_{Rx_1}^{M_1}\right\}, \tag{23}$$

$$TOA_{Rx_2}(\tau_k) = \left\{TOA_{Rx_2}^1, TOA_{Rx_2}^2, \cdots TOA_{Rx_2}^{M_2}\right\}, \tag{24}$$

where $TOA_{Rx_i}^m$ is the TOA of the m-th target confirmed by the i-th receiving channel. M_1 and M_2 represents the number of the confirmed targets for which TOA has been estimated by the first and second receiving channels, respectively.

As follows from target localization theory, for a target localization by a radar according to (6), a pair of TOAs

$$\left\{TOA_{Rx_1}^m(\tau_k), TOA_{Rx_2}^n(\tau_k)\right\} \tag{25}$$

associated with the same target has to be used. Using (23) and (24), M_1 M_2 such pairs can be created, and hence theoretically, M_1 M_2 targets could be localized. However, if e.g., $M_1 \geq M_2$, then maximum M_2 valid targets could be in the monitored area only, while the remaining $M_1 M_2 - M_2$ potential targets are so-called ghosts. And hence, to localize valid targets situated in the monitored area, $M_3 \leq M_2$ pairs of TOAs according to (25) associated with the same target have to be selected. The trace connection method also provides a solution to this TOA association task. Then, the result of the currently discussed phase of the SPL is given by a set of $M_3 \leq M_2$ pairs of TOA according to (25) that are correctly associated. For simplicity, in the next the associated TOAs of the p-th target will be denoted as $TOA_{Rx_i}^p$ for $p \in M_3, i = 1, 2$.

E. Wall Effect Compensation

In the case of SP localization for LOS scenarios, the target TOAs are estimated using the trace connection method. Then, target bistatic distances can be computed by (3). And finally, these distances are employed to localize the target [42]. Now let us consider SP localization for TW scenarios. For such scenarios, the target could be localized in the same way as for LOS scenarios. However, in this case, the target position will be estimated with an error usually larger than that for LOS scenarios. The mentioned growth of the localization error is caused by the fact, that the velocity of electromagnetic wave propagation in the wall is lower than in the air. In the field of the person monitoring by UWB radars, this effect is referred to as the wall effect [42], [48]. The range of the impact of the wall effect depends on the wall properties (such as its thickness, profile, permittivity, and permeability), and on the ratio of the wall thickness and the distance traveled by electromagnetic waves in the air.

To improve the person localization accuracy for TW scenarios, the methods of the wall effect compensation can be used [42], [48]. These methods are based on the estimation of time delay t_d caused by the transmission of the electromagnetic wave through the wall. The estimated time delay is applied for TOA correction by using the expression

$$T_{Rx_i}^p(\tau_k) = TOA_{Rx_i}^p(\tau_k) - t_d. \tag{26}$$

Then, the TOAs corrected according to (26) are used for the target localization.

For the wall effect compensation, two methods referred to as target trace correction of the 1st and 2nd kind have been proposed in [42], [48]. Both methods use (26) but differ in the way how t_d is estimated. For example, in the case of the target trace correction of the 1st kind

$$t_d = \frac{d_W}{c}\left(\sqrt{\epsilon_r \mu_r} - 1\right) \tag{27}$$

where d_W, ϵ_r, and μ_r are the wall thickness, permittivity, and permeability of the wall material. The method of the trace correction of the 2nd kind is able to provide better performance, but is also more complex. Besides the mentioned methods, more advanced approaches (usually used in ground penetrating radar field) can be found e.g. in [49]–[51].

For LOS scenarios, $\epsilon_r = 1$ and $\mu_r = 1$, and hence $t_d = 0$. Then, the following expression can be formally written

$$T^p_{Rx_i}(\tau_k) = TOA^p_{Rx_i}(\tau_k). \tag{28}$$

If the target TOAs are expressed by $T^p_{Rx_i}(\tau_k)$, then in the target localization phase the velocity of the electromagnetic wave propagation in the air $c = 3 \times 10^8$ ms^{-1} has to be considered.

F. Target Localization

Let the antenna array of the radar consists of 1 Tx and 2 Rx, while the coordinates of the particular antennas are given by (6). Suppose further that for the observation time instant τ_k the pair of the corrected TOAs associated with the p-th target $T^p_k = \left(x^p_k, y^p_k\right)$ situated in the $x - y$ plane for $y > 0$ are known, and are given by the expression

$$\left\{T^p_{Rx_1}(\tau_k), T^p_{Rx_2}(\tau_k)\right\}. \tag{29}$$

Then the target localization phase aims to determine the coordinates of T^p_k denoted as x^p_k and y^p_k.

Using (3), (6), and (28), we can write the following equations

$$d_i(\tau_k) = cT^p_{Rx_i}(\tau_k) \text{ for } i = 1, 2, \tag{30}$$

$$\begin{aligned} d_i(\tau_k) &= \left\|TxT^p_k\right\| + \left\|Rx_iT^p_k\right\| \\ &= \sqrt{\left(x^p_k\right)^2 + \left(y^p_k\right)^2} + \sqrt{\left(x^p_k - x_i\right)^2 + \left(y^p_k - y_i\right)^2}, \end{aligned} \tag{31}$$

where $d_i(\tau_k)$ is the i-th bistatic distance of the target T^p_k.

It has been shown e.g. in [52] that the solution of (31) can be found in the form

$$x^p_k = \frac{d_1k_2 - d_2k_1}{d_2x_1 - d_1x_2}, \tag{32}$$

$$y^p_k = \sqrt{\left(\frac{k_1 + x_1x^p_k}{d_1}\right)^2 - \left(x^p_k\right)^2}, \quad y^p_k \geq 0, \tag{33}$$

where

$$k_i = \frac{1}{2}\left(d_i^2 - x_i^2\right), \; d_i = d_i(\tau_k) \text{ from (30) for } i = 1, 2. \tag{34}$$

The analysis of (31) has shown, that it can have 0, 1, or 2 solutions. The situation where (31) has 0 or 1 solution indicates that the target $T^p_k = \left(x^p_k, y^p_k\right)$ cannot be localized. If two solutions of (31) exist, then target coordinates are given by (32) and (33). The second solution $T^{p\prime}_k = \left(x^p_k, -y^p_k\right)$ can be excluded because is located behind the radar antennas.

The described approach to the target localization is usually referred to as the direct localization method [52]. Using this method, the coordinates of all targets for all possible associated pairs of TOAs are computed. The result of the localization phase is then given by the set of all localized targets

$$O(\tau_k) = \left\{T^p_k = \left(x^p_k, y^p_k\right) \text{ for } p = 1, 2, \cdots, M_3(\tau_k)\right\}. \tag{35}$$

The results of the localization phase expressed by $T^p_k = \left(x^p_k, y^p_k\right)$ are usually referred to as observations [53].

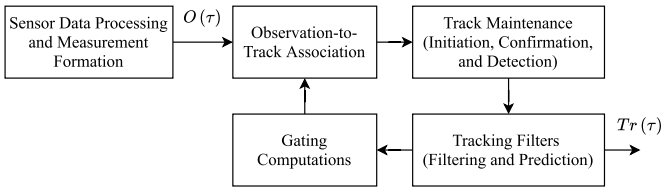

Fig. 3. MTT system.

G. Target Tracking

The target tracking phase of SPL is used to associate consecutive radar observations of the same targets into target tracks. In contrast to localization, tracking also provides a new recursive estimation of the target location based on its current and foregoing observations and thus it decreases the target coordinate estimation error. As SPL has to track multiple targets, we propose to use a multiple target tracking system (MTT) for SP tracking. MTT is a complex system of radar observation processing that has to handle basic multiple-target tracking problems such as target tracking itself, target-to-track association, missing observations, false alarms, and track maintenance [53].

Because there are many algorithms to solve the mentioned partial tasks of MTT, there are also a lot of concepts, variants, and modifications of MTT [53]. We have chosen for SPL a classic MTT system shown in Fig. 3 [42]. Its input in the observation time instant τ_k is given by the set of observations $O(\tau_k)$ from (35). On the other hand, its output is represented by the set of the target tracks

$$TR(\tau_k) = \left\{TR^r_k \text{ for } r = 1, 2, \cdots, M_4(\tau_k)\right\}, \tag{36}$$

where TR^r_k is the r-th track obtained in the observation time instant τ_k. The number of tracks $M_4(\tau_k)$ may differ from the number of observations $M_3(\tau_k)$.

A detailed description of the MTT proposed for SPL is too complex to be presented in this paper (for detailes see [42], [53], [54]). Therefore, in the following, we will present only its brief overview.

It is well known that any target tracking in the presence of clutter and multiple targets requires that proper observations be assigned to each target track by comparing them with the corresponding predicted observation positions. In our MTT, it is implemented by the combination of observation gating with Munkres algorithm (target-to-track association algorithm). The observation prediction and the gate size are usually provided by the tracking filters. In the MTT used by SPL, for observation prediction and track updates, a set of linear Kalman filters with a constant velocity model are employed. When the velocity of the target is significantly decreased, which indicates that the target probably stopped, the parameter controlling the gate size is decreased and vice versa. In such a way, the same model for MP and SP tracking can be used with a computational advantage. The observation gating also supports the suppression of false alarms. On the other hand, the problem of missing observations can be solved using the observation prediction. The track maintenance represents the last block of MTT given in Fig. 3. It includes track initiation, confirmation,

and deletion. In the MTT used by SPL, it is implemented by so-called M/N logic.

SP tracking is a beneficial feature of the signal processing schemes applied to SP localization which is not used in common (we outlined its usage in [18] and [19]). Its main positive contribution is improvement of the accuracy of SP localization and reduction of the relative frequency of false alarms, as well as handling of the problem of short-term missing observations. On the other hand, the MTT application indeed increases the computational complexity of the SPL. Compared to other approaches to SP localization mentioned in Section II, the complexity of SPL is significantly reduced by the fact that SPL does not use any BS-M. Moreover, as is mentioned in Section III, the SPL introduced in this paper should be able to be used effectively as a part of signal processing schemes for MP-SP monitoring. In such a case, the same MTT (as described above) can be used for tracking not only SP but MP as well. Therefore, the proposed use of MTT under SPL can be considered acceptable in view of its computational complexity.

V. Experimental Results

This section aims to present the performance properties of the SPL. To demonstrate the robustness of SPL we have included in this section the experimental results of LOS and TW scenario as well. With the same focus, different radars, namely passband, and baseband operating radar were applied in the considered scenarios.

A. LOS Localization of Two SPs

The first scenario referred to as LOS scenario was focused on LOS in-door localization of two SPs situated in an office. The scenario measurement scheme is shown in Fig. 4. Person A (B) was situated during the whole measurement at the position P_1 (P_2). During the measurement running on 48 s, the persons to be localized performed only respiratory movements. The persons were monitored by a multistatic M-sequence UWB radar satisfying the standard of the European Electronic Communications Committee (ECC radar) [40]. The parameters of the ECC radar and its antennas are summarized in Table I. The radar antenna array consisted of one Tx and two Rx placed up in the corner of the office. Here, Tx was located in the middle between Rx_1 and Rx_2.

For SP localization and tracking, the SPL described above was applied. Within the phase of raw data preprocessing, synchronous averaging by factor 3072 was used. Because the measurement rate was 13857.63 impulse responses per second (IR/s), the sampling frequency along the τ-axis was $f_\tau = 4$ Hz. As the range filter, the zero-phase elliptical filter of the 8th order with cut-off frequencies of the pass-band $f_L = 6$ GHz and $f_U = 8.5$ GHz was employed.

The outputs of the selected phases of SPL obtained for the LOS scenario are shown in Fig. 5–16, Table II, and Table III. In Fig. 5–10, we can observe the results of the processing of signals received by Rx_1. Because similar results were obtained for Rx_2, they are not reported here, but they were used for target localization.

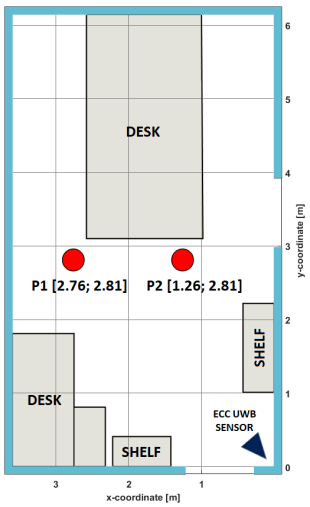

Fig. 4. The measurement scheme. LOS scenario.

TABLE I
ECC Radar System Parameters

M-sequence order	9
Clock frequency	10.8768 GHz
Signal bandwidth	6.0 – 8.5 GHz
Length of impulse responses	1533 samples
Radar range resolution	0.0276 m
Maximum unambiguous range of radar	21.13 m
Radar measurement rate	13857.63 IR/s
Number of hardware synchronously averaged scans	48
Number of software synchronously averaged scans	8
Sampling frequency along the τ-axis	4.419 Hz (after averaging)
Antenna spacing	0.1 m
Antenna type	Custom frame antennas operating in the frequency band 6 GHz – 8.5 GHz
Transmitted power	6 dBm

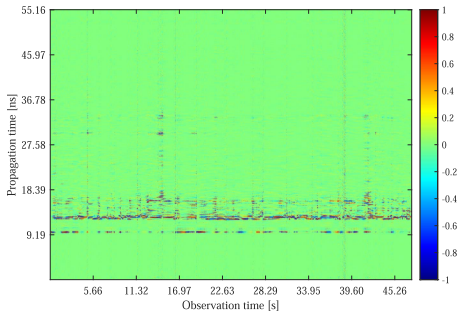

Fig. 5. The radargram with the subtracted background. LOS scenario. Rx_1.

After the raw data preprocessing, the radargram consisting of the resampled and synchronous averaged radar scans filtered by the range filter is obtained. Its high-level components correspond mainly to the coupling between antennas. As the $ENCR$ is too low, no target echoes can be visible there. The level of $ENCR$ has been increased by background subtracting

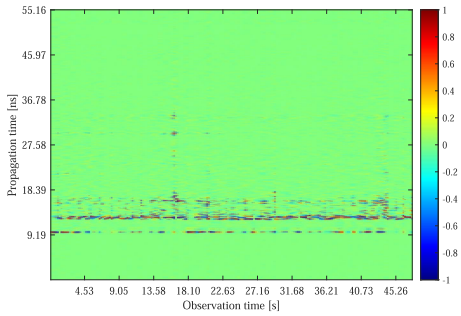

Fig. 6. The τ-filter output. LOS scenario. Rx_1.

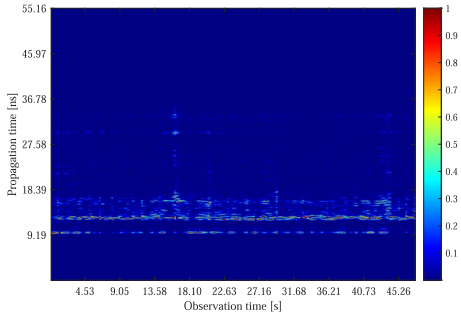

Fig. 7. Estimation of $P(t, \tau)$. LOS scenario. Rx_1.

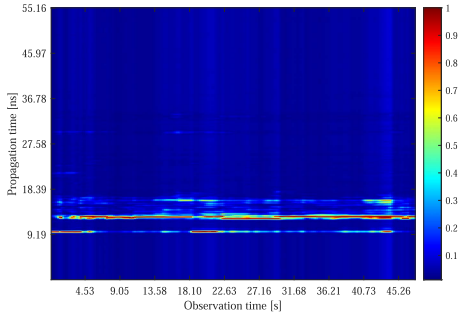

Fig. 8. $e_{RMS}(t, \tau)$. LOS scenario. Rx_1.

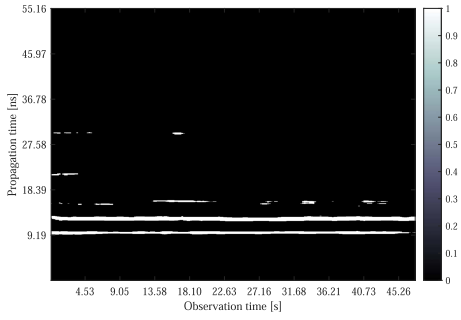

Fig. 9. OS-CFAR output. LOS scenario. Rx_1.

and τ-filtering. Then, the target echoes can be identified in Fig. 5-6 around $TOA_A \approx 15$ ns (person A) and $TOA_B \approx 9.25$ ns (person B). Unfortunately, besides the target echo components, some additional high-level signal artifacts can be observed in these figures. They originate, mainly in the multipath propagation of electromagnetic waves, as well as in the target micro-motion.

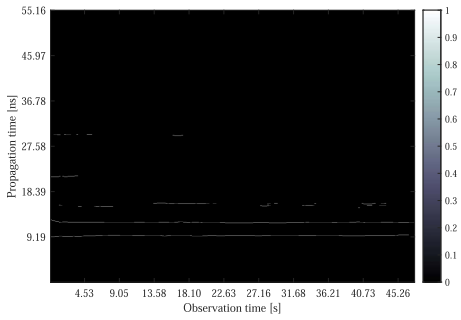

Fig. 10. Threshold detector output. LOS scenario. Rx_1.

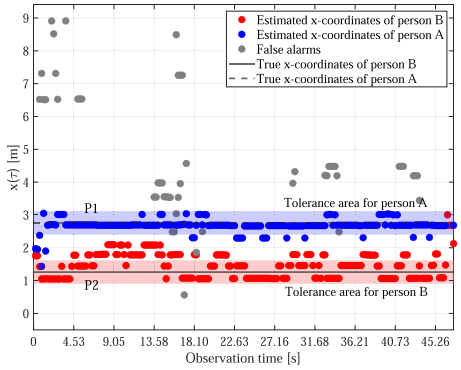

Fig. 11. Target localization. The estimates of *x*-coordinates of the targets. LOS scenario.

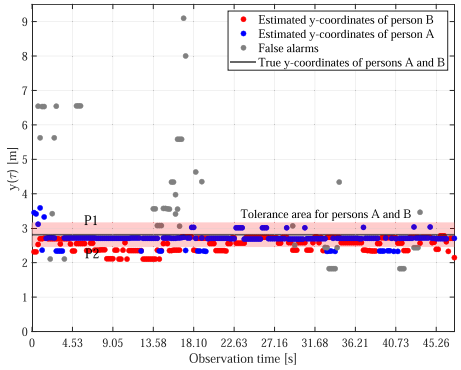

Fig. 12. Target localization. The estimates of *y*-coordinates of the targets. LOS scenario.

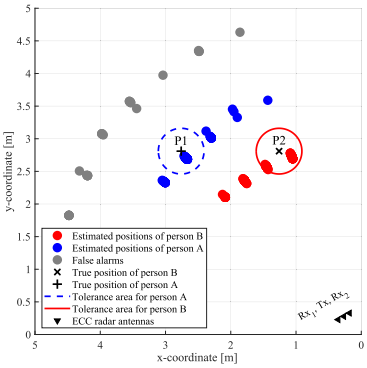

Fig. 13. Target localization in the $x - y$ plane. LOS scenario.

Fig. 6-8 illustrate how testing statistics of the detector are gradually formed. In these figures, we see not only $P(t, \tau)$ and $e_{RMS}(t, \tau)$ components originating in the target echoes, but

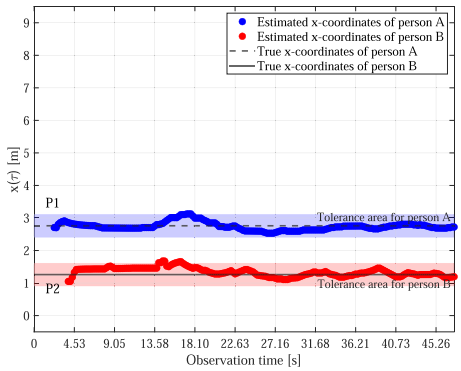

Fig. 14. Target tracking. The estimates of *x*-coordinates of the targets. LOS scenario.

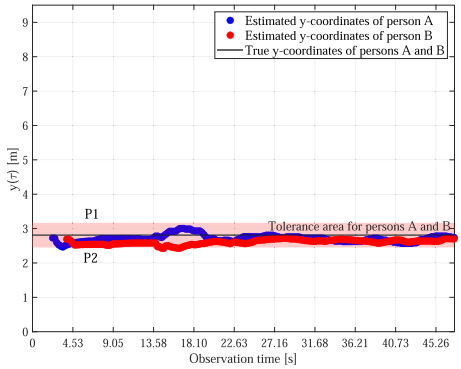

Fig. 15. Target tracking. The estimates of *y*-coordinates of the targets. LOS scenario.

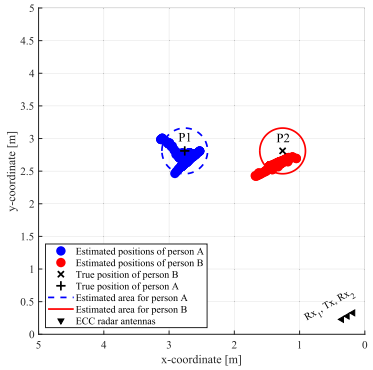

Fig. 16. Target tracking in the $x-y$ plane. LOS scenario.

also their components derived from the high-level signal artifacts mentioned in the previous paragraph. These components have resulted in false alarms shown in Fig. 9 and Fig. 10. However, what is important, in Fig. 9 and Fig. 10 we also see the components of the detector response corresponding to persons A and B.

Using estimated and associated TOAs, the potential targets have been localized. The true and the estimated x and $y-$coordinates of the targets vs. observation time are shown in Fig. 11 and Fig. 12. Moreover, the true and estimated positions of persons A and B obtained as the localization phase output and observed during the whole measurement are displayed in Fig. 13. We can see from these figures that x and $y-$coordinates and the positions of the targets are concentrated

TABLE II
QUANTITATIVE ANALYSIS OF EXPERIMENTAL RESULTS. TARGET LOCALIZATION. LOS SCENARIO

	Person A	Person B
Mean of $e_x(\tau)$ [m]	0.3541	0.1406
Standard deviation of $e_x(\tau)$ [m]	0.2498	0.1607
$max\left[e_x(\tau)\right]$ [m]	1.7438	1.3274
Mean of $e_y(\tau)$ [m]	0.2758	0.1663
Standard deviation of $e_y(\tau)$ [m]	0.1953	0.1371
$max\left[e_y(\tau)\right]$ [m]	0.7067	0.7798
Mean of $e_T(\tau)$ $(\bar{e}_T^L)$ [m]	0.4574	0.2237
Standard deviation of $e_T(\tau)$ (σ_T^L) [m]	0.3046	0.2049
$max\left[e_T(\tau)\right]$ [m]	1.8094	1.5396
Relative frequency of the correct estimation $x(\tau)$ [%]	90.78	63.16
Relative frequency of the correct estimation $y(\tau)$ [%]	86.41	66.44
Relative frequency of the correct localization of a target [%]	79.13	63.16

TABLE III
QUANTITATIVE ANALYSIS OF EXPERIMENTAL RESULTS. TARGET TRACKING. LOS SCENARIO

	Person A	Person B
Mean of $e_x(\tau)$ [m]	0.1201	0.0952
Standard deviation of $e_x(\tau)$ [m]	0.0946	0.0817
$max\left[e_x(\tau)\right]$ [m]	0.4188	0.3657
Mean of $e_y(\tau)$ [m]	0.2039	0.1222
Standard deviation of $e_y(\tau)$ [m]	0.0680	0.0682
$max\left[e_y(\tau)\right]$ [m]	0.3876	0.3454
Mean of $e_T(\tau)$ $(\bar{e}_T^L)$ [m]	0.2439	0.1745
Standard deviation of $e_T(\tau)$ (σ_T^T) [m]	0.1003	0.0696
$max\left[e_T(\tau)\right]$ [m]	0.5668	0.4062
Relative frequency of the correct estimation $x(\tau)$ [%]	95.34	98.50
Relative frequency of the correct estimation $y(\tau)$ [%]	96.37	100
Relative frequency of the correct localization of a target [%]	88.08	96.5

around their true values, but there are also some relatively large deviations among true and estimated values of coordinates and positions. The distribution of the individual observations in the $x-y$ plane shown in Fig. 13 is caused not only by the error of the TOA estimation but is mainly the result of the effect of geometric dilution of precision [55]. Moreover, some false targets and missing targets can be visible in these figures. This is the reason why the tracking phase has been incorporated in the SPL.

The results of the target tracking are shown in Fig. 14 - 16. Similar to the case of the localization phase, we can see in these figures the true and estimated coordinates, and positions of the persons to be tracked in $x-y$ plane. The comparison of Fig. 11 - 16 shows that the tracking application has allowed to significantly improve the accuracy of the target localization. As we can observe in these figures, the accuracy of the target location provided by the tracking phase is very good, with no false target found. In addition, the target tracks were formed relatively quickly, approximately 4 s after the start of the measurement. Finally, no missing targets were observed after the creation of the track.

To provide a quantitative analysis of the results obtained for the LOS scenario, we have created tolerance areas around the true values of the target coordinates and the true position of the targets in the $x-y$ plane. The tolerance area for a true value of a target coordinate is given by a planar strip drawn symmetrically around the true value of a target coordinate. The width of the strip is $2\Delta_W$, which corresponds approximately to the diameter of a human chest. On the other hand, in the $x-y$ plane, the tolerance area is expressed by a circle with the centre in the true position of the target and with the diameter $2\Delta_W$. All possible tolerance areas created for the LOS scenario are shown in Fig. 11-16. Because SPs are not pointed but distributed targets, with no-zero size and because the size of the proposed tolerance areas is comparable with the size of SP, it is clear that if the estimated coordinates or position of SPs are situated inside of the tolerance area, then the accuracy of estimation of coordinates or position of SP can be considered very good.

Let C_T and C_E represent the true and estimated coordinates of a target for $C\epsilon\{x, y\}$, and let $T_T = (x_T, y_T)$ and $T_E = (x_E, y_E)$ be the true and estimated target position given by its coordinates in the $x-y$ plane. Then, the estimation error of coordinate C ($e_C(\tau)$) and estimation error of localization ($e_T(\tau)$) of a target are given by

$$e_C(\tau) = |C_T(\tau) - C_E(\tau)|, \tag{37}$$

$$e_T(\tau) = \|T_T(\tau)\, T_E(\tau)\| = \sqrt{(x_T(\tau) - x_E(\tau))^2 + (y_T(\tau) - y_E(\tau))^2}. \tag{38}$$

Then, an estimated coordinate of the target C_E and the estimated position of the target are situated in its tolerance area if it holds

$$e_C(\tau) \leq \Delta_W, \tag{39}$$

$$e_T(\tau) \leq \Delta_W. \tag{40}$$

If (39) and (40) hold, then we talk about a correct estimate of the coordinate and a correct estimate of the position of the target.

Using the true and estimated coordinates of person A and B, as well as (37)-(40), we can evaluate the accuracy of the target localization and tracking using the set of quantitative characteristics shown in Table II and Table III. The comparison of data presented there illustrate the contribution of the tracking phase to the accuracy of the final target localization. For example, the mean values and standard deviations of the target localization errors obtained at the output of the target localization phase take on values $\bar{e}_T^L(A) = 0.4574$ m, $\sigma_T^L(A) = 0.3046$ m for person A, and $\bar{e}_T^L(B) = 0.2237$ m, $\sigma_T^L(B) = 0.2049$ m for person B respectively. In contrast, these parameters obtained at the output of the target tracking phase take on values $\bar{e}_T^T(A) = 0.2439$ m, $\sigma_T^T(A) = 0.1003$ m, $\bar{e}_T^T(B) = 0.1745$ m, and $\sigma_T^T(B) = 0.0696$ m. It confirms that target tracking is a very strong tool of SPL that significantly improves the accuracy of SP localization. As follows from Table III, the SPL provides the SP localization with very good accuracy at a relatively short time (4 s) necessary for the target track creation.

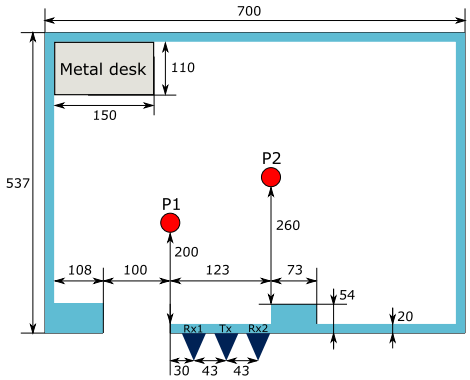

Fig. 17. The measurement scheme. The distances are in cm.

B. TW Localization of SPs

The second scenario was focused on TW localization of persons (TW scenario) with a changing number of people located in the monitored area. The measurement scheme is shown in Fig. 17. Here, the distances are in cm. The thickness of a brick wall through which SPs were monitored was 20 cm. The particular positions and the presence of the persons to be localized within the experimental scenario can be split into the phases:

- A: Time interval of measurement $T_A = \langle 0\text{ s}, 65\text{ s}\rangle$: Person A (B) was standing in position P_2 (P_1) for 65 s.
- B: Time interval of measurement $T_B = \langle 65\text{ s}, 75\text{ s}\rangle$: Person A was standing in position P_2 for 10 s. Person B was leaving the monitored area.
- C: Time interval of measurement $T_C = \langle 75\text{ s}, 120\text{ s}\rangle$: Person A was standing in position P_2 for 45 s. Person B was not present in the monitored area.
- D: Time interval of measurement $T_D = \langle 120\text{ s}, 130\text{ s}\rangle$: Person A was standing in position P_2 for 10 s. Person B entered the monitored area and returned back at position P_1.
- E: Time interval of measurement $T_E = \langle 130\text{ s}, 195\text{ s}\rangle$: Person A(B) was standing in position P_2 (P_1) for 65 s.

Within this scenario, a baseband M-sequence UWB radar was employed (TW radar) [56], [57]. The parameters of the TW radar and its antennas are summarized in Table IV. The radar antenna array consisted of 1 Tx and 2 Rxs. The antenna array layout and its position in the monitored area are outlined in Fig. 17.

For SP localization and tracking, the SPL described above was applied. Within the phase of raw data preprocessing, synchronous averaging by factor 1536 was used. As the measurement rate was 6349.2 IR/s, the sampling frequency along the τ-axis was $f_\tau = 4.0492$ Hz. The range filtering was not implemented in the TW scenario.

To respect the reasonable range of the contribution, we present for the TW scenario only the results of the tracking phase (Fig. 18–20) and the evaluation of the accuracy of the target tracking by the quantitative characteristics (Table V). Qualitative analysis of the results of other phases of the SPL would lead to the same conclusions as those for LOS scenario.

In Fig. 18–20, we can see the true and estimated coordinates, and positions of the persons to be tracked in the

TABLE IV
TW RADAR SYSTEM PARAMETERS

M-sequence order	12
Clock frequency	13.312 GHz
Signal bandwidth	DC – 6.3 GHz
Length of impulse responses	4095 samples
Radar range resolution	0.0225 m
Maximum unambiguous range of radar	46.11 m
Radar measurement rate	6349.2 IR/s
Number of hardware synchronously averaged scans	48
Number of software synchronously averaged scans	8
Sampling frequency along the τ-axis	4.0492 Hz (after decimation (averaging))
Antenna spacing	0.43 m
Antenna type	Horn antennas operating in the frequency band 740 MHz – 10.5 GHz (type DRH10) [58])
Transmitted power	10 dBm

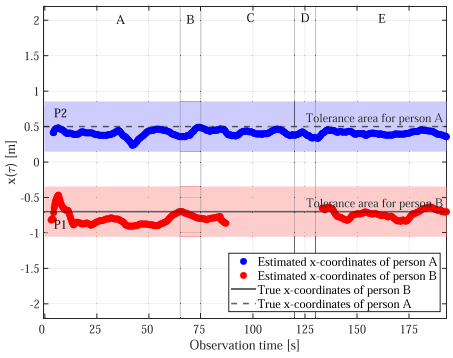

Fig. 18. Target tracking. The estimates of *x*-coordinates of the targets. TW scenario.

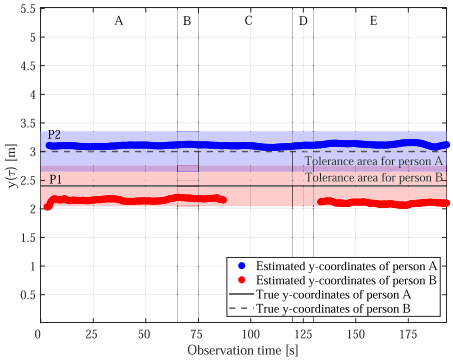

Fig. 19. Target tracking. The estimates of *y*-coordinates of the targets. TW scenario.

$x - y$ plane. Similar to the LOS scenario, the SPL has formed the target tracks, approximately 4 s after the start of the measurement. During phases B-D of the TW scenario, person B is in the role of MP, or person B is not present in the monitored area. Therefore, during these phases person B should not be detected and tracked by the SPL. As we can observe from Fig. 18–20, the track of person B was deleted at the observation time instant 88 s, i.e. approximately 12 s after person B has changed his role from the SP to the role of MP.

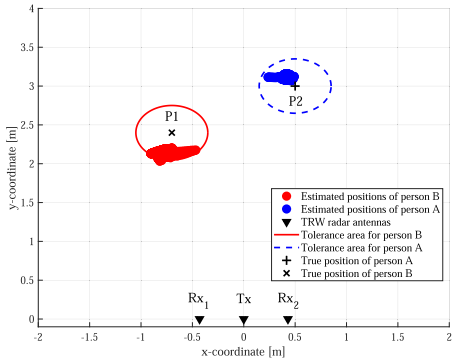

Fig. 20. Target tracking in the $x - y$ plane. TW scenario.

TABLE V
QUANTITATIVE ANALYSIS OF EXPERIMENTAL RESULTS. TARGET TRACKING. TW SCENARIO

	Person A	Person B
Mean of $e_x(\tau)$ [m]	0.0932	0.0939
Standard deviation of $e_x(\tau)$ [m]	0.0396	0.0606
$max[e_x(\tau)]$ [m]	0.2643	0.2337
Mean of $e_y(\tau)$ [m]	0.1105	0.2657
Standard deviation of $e_y(\tau)$ [m]	0.0195	0.0361
$max[e_y(\tau)]$ [m]	0.1582	0.3666
Mean of $e_T(\tau)$ ($\bar{e}_T^L$) [m]	0.1480	0.2879
Standard deviation of $e_T(\tau)$ (σ_T^T) [m]	0.0306	0.0386
$max[e_T(\tau)]$ [m]	0.2878	0.3849
Relative frequency of the correct estimation $x(\tau)$ [%]	98.06	97.7
Relative frequency of the correct estimation $y(\tau)$ [%]	98.06	96.66
Relative frequency of the correct localization of a target [%]	100	96.6

The new track for person B was created at the observation time instant 134 s, i.e. approximately 4 s after returning person B to position P_1. Both delays (first deletion and then the creation of B person track) were due to MTT (inertia of algorithms focused on track maintenance) are, according to our opinion, fully acceptable. These results have outlined that the SPL has the potential to handle scenarios with a changing number of people situated in the monitored area. We have not addressed the issue of person B tracking if he is in the role of MP (B and D phases) because the solution of this issue is beyond this paper. Some starting points for solving the mentioned problem are indicated e.g., in [4].

Quantitative analysis of the experimental results obtained for the TW scenario is shown in Table V. As follows from this table the mean value and standard deviation of the target localization error obtained at the output of the target tracking phase take on values $\bar{e}_T^T(A) = 0.1480$ m, $\sigma_T^T(A) = 0.0306$ m for the person A, and $\bar{e}_T^T(B) = 0.2879$ m, $\sigma_T^T(B) = 0.0386$ m for person B respectively. These results confirm that SPL allows for reaching good accuracy of the SP localization also for scenarios focused on multiple SP localization with a changing number of people located in the monitored area.

VI. CONCLUSION

In this paper, we have introduced a new approach to SP localization and tracking referred to as SPL.

Firstly, we proposed to sample the raw radar data along the τ-axis with the frequency $f_\tau \approx 4$ Hz. The use of such sampling frequency is very helpful since it reduces the requirements for computing resources applied for SPL real-time implementation.

Then we have introduced SPL itself as the complex of seven signal processing phases. The SPL is characterized by the fact that its phases are implemented only by SS-M. As result, the output of SPL is generated at the same rate as the sampling frequency of the radar resampled scans (f_τ) is. This concept, supplemented by the target tracking phase, enables the effective combination of SPL with MP localization methods, and thus allows for creating new effective MP-SP localization methods. In addition, the SS-M only application reduces the overall computational complexity of SPL. Other new features of the SPL are the new approach to SP detection and the inclusion of SP tracking in the SPL. As we have shown by experimental results, these solutions have contributed effectively to the very good performance of the SPL. The proposed SPL also allows monitoring of multiple persons including scenarios where the number of persons is changing.

The performance properties of SPL illustrated by the experimental results have confirmed that SPL provides very good performance for LOS and TW scenarios as well as for different types of radars. The same performance of SPL has been obtained for its real-time implementation. As the SPL is based on the processing of impulse responses measured by radar, it can be directly used for SP localization by means of any UWB radar measuring such impulse responses (e.g., impulse UWB radar).

As we have shown above, the SPL introduced in this paper possesses all properties requested in Section III. Therefore, we believe it could be a useful and efficient tool for human monitoring for many application scenarios.

REFERENCES

[1] R. F. Brena, J. P. García-Vázquez, C. E. Galván-Tejada, D. Munoz-Rodriguez, C. Vargas-Rosales, and J. Fangmeyer, "Evolution of indoor positioning technologies: A survey," *J. Sens.*, vol. 2017, pp. 1–21, Mar. 2017.

[2] D. Kocur, J. Rovňáková, and M. Švecová, "Through wall tracking of moving targets by M-sequence UWB radar," in *Towards Intelligent Engineering and Information Technology*, I. J. Rudas, J. Fodor, and J. Kacprzyk, Eds. Berlin, Germany: Springer, 2009, pp. 349–364.

[3] D. Novák, M. Švecová, and D. Kocur, "Multiple person localization based on their vital sign detection using UWB sensor," in *Microwave Systems and Applications*, S. Goudos, Ed. Rijeka, Croatia: InTech, 2017.

[4] M. Švecová and D. Kocur, "Localization of a person moving with an unknown character of motion," *J. Electromagn. Waves Appl.*, vol. 35, no. 5, pp. 647–671, Mar. 2021.

[5] D. Kocur and M. Svecova, "Signal processing for monitoring of static persons using UWB sensors: A survey," in *IEEE MTT-S Int. Microw. Symp. Dig.*, vol. 1, May 2019, pp. 1–3.

[6] J. Sachs, *Handbook of Ultra-Wideband Short-Range Sensing: Theory, Sensors, Applications*. Hoboken, NJ, USA: Wiley, 2013.

[7] M. Corrigan, A. Walton, W. Niu, J. Li, and T. Talty, "Automatic UWB clusters identification," in *Proc. IEEE Radio Wireless Symp.* New York, NY, USA: IEEE Press, Jan. 2009, pp. 363–366.

[8] A. A. M. Saleh and R. Valenzuela, "A statistical model for indoor multipath propagation," *IEEE J. Sel. Areas Commun.*, vol. JSAC-5, no. 2, pp. 128–137, Feb. 1987.

[9] M. Lee and J.-Y. Lee, "Statistical modeling of indirect paths for UWB sensors in an indoor environment," *Sensors*, vol. 17, no. 12, p. 43, Dec. 2016.

[10] A. Lazaro, D. Girbau, and R. Villarino, "Analysis of vital signs monitoring using an IR-UWB radar," *Prog. Electromagn. Res.*, vol. 100, pp. 265–284, Jan. 2010.

[11] J. Sachs, M. Helbig, R. Herrmann, M. Kmec, K. Schilling, and E. Zaikov, "Remote vital sign detection for rescue, security, and medical care by ultra-wideband pseudo-noise radar," *Ad Hoc Netw.*, vol. 13, pp. 42–53, Feb. 2014.

[12] A. Lazaro, D. Girbau, and R. Villarino, "Techniques for clutter suppression in the presence of body movements during the detection of respiratory activity through UWB radars," *Sensors*, vol. 14, no. 2, pp. 2595–2618, Feb. 2014.

[13] A. Nezirovic, "Trapped-victim detection in post-disaster scenarios using ultra-wideband radar," Ph.D. dissertation, Int. Res. Centre Telecommun. Radar, Delft Univ. Technol., Delft, The Netherlands, 2010.

[14] A. Singh, S. U. Rehman, S. Yongchareon, and P. H. J. Chong, "Multi-resident non-contact vital sign monitoring using radar: A review," *IEEE Sensors J.*, vol. 21, no. 4, pp. 4061–4084, Feb. 2021.

[15] (Feb. 2019). *What Is a Normal Respiratory Rate?* [Online]. Available: https://www.medicalnewstoday.com/articles/324409

[16] A. Nezirovic, A. G. Yarovoy, and L. P. Ligthart, "Signal processing for improved detection of trapped victims using UWB radar," *IEEE Trans. Geosci. Remote Sens.*, vol. 48, no. 4, pp. 2005–2014, Apr. 2010.

[17] C. Kim and J.-Y. Lee, "ToA-based multi-target localization and respiration detection using UWB radars," *EURASIP J. Wireless Commun. Netw.*, vol. 2014, no. 1, pp. 1–15, Dec. 2014.

[18] D. Kocur, T. Porteleky, and M. Švecová, "UWB radar testbed system for localization of multiple static persons," in *Proc. IEEE SENSORS*, Oct. 2019, pp. 1–4.

[19] M. Švecová, T. Porteleky, and D. Kocur, "Real-time operating UWB sensor system for static person localization," in *Proc. Photon. Electromagn. Res. Symp. Spring (PIERS-Spring)*, Jun. 2019, pp. 3558–3565.

[20] J.-E. Kim, J.-H. Choi, and K.-T. Kim, "Robust detection of presence of individuals in an indoor environment using IR-UWB radar," *IEEE Access*, vol. 8, pp. 108133–108147, 2020.

[21] S. Singh, Q. Liang, D. Chen, and L. Sheng, "Sense through wall human detection using UWB radar," *EURASIP J. Wireless Commun. Netw.*, vol. 2011, no. 1, pp. 1–11, Dec. 2011.

[22] X. Li, Q. Liang, and F. C. M. Lau, "Sense-through-wall human detection using the UWB radar with sparse SVD," *Phys. Commun.*, vol. 13, pp. 260–266, Dec. 2014.

[23] J. Li, L. Liu, Z. Zeng, and F. Liu, "Simulation and signal processing of UWB radar for human detection in complex environment," in *Proc. 14th Int. Conf. Ground Penetrating Radar*, 2012, pp. 209–213.

[24] L. Qiu, T. Jin, J. Zhang, B. Lu, and Z. Zhou, "An iterative singular vector decomposition based micro-motion target indication in through-the-wall radar," in *Proc. IEEE Int. Geosci. Remote Sens. Symp. (IGARSS)*, Jul. 2016, pp. 6597–6600.

[25] J. Li, L. Liu, Z. Zeng, and F. Liu, "Advanced signal processing for vital sign extraction with applications in UWB radar detection of trapped victims in complex environments," *IEEE J. Sel. Topics Appl. Earth Observ. Remote Sens.*, vol. 7, no. 3, pp. 783–791, Mar. 2014.

[26] J.-H. Choi, J.-E. Kim, and K.-T. Kim, "People counting using IR-UWB radar sensor in a wide area," *IEEE Internet Things J.*, vol. 8, no. 7, pp. 5806–5821, Apr. 2020.

[27] A. Kumar, Z. Li, Q. Liang, B. Zhang, and X. Wu, "Experimental study of through-wall human detection using ultra wideband radar sensors," *Measurement*, vol. 47, pp. 869–879, Jan. 2014.

[28] Z. Liu, L. Liu, and B. Barrowes, "The application of the Hilbert-Huang transform in through-wall life detection with UWB impulse radar," *PIERS Online*, vol. 6, no. 7, pp. 695–699, 2010.

[29] N. E. Huang *et al.*, "The empirical mode decomposition and the Hilbert spectrum for nonlinear and non-stationary time series analysis," *Proc. Roy. Soc. London A, Math., Phys. Eng. Sci.*, vol. 454, no. 1971, pp. 903–995, Mar. 1998.

[30] J. Li, Z. Zeng, J. Sun, and F. Liu, "Through-wall detection of human being's movement by UWB radar," *IEEE Geosci. Remote Sens. Lett.*, vol. 9, no. 6, pp. 1079–1083, Nov. 2012.

[31] X. Liang, H. Zhang, T. Lyu, L. Xu, C. Cao, and T. A. Gulliver, "Ultra-wide band impulse radar for life detection using wavelet packet decomposition," *Phys. Commun.*, vol. 29, pp. 31–47, Aug. 2018.

[32] Y. Wang *et al.*, "Using wavelet entropy to distinguish between humans and dogs detected by UWB radar," *Prog. Electromagn. Res.*, vol. 139, pp. 335–352, Jan. 2013.

[33] Y. Xu, S. Dai, S. Wu, J. Chen, and G. Fang, "Vital sign detection method based on multiple higher order cumulant for ultrawideband radar," *IEEE Trans. Geosci. Remote Sens.*, vol. 50, no. 4, pp. 1254–1265, Apr. 2012.

[34] C. in *et al.*, "Human detection based on the condition number in the non-stationary clutter environment using UWB impulse radar," in *Proc. Asia–Pacific Microw. Conf. Proc. (APMC)*, Nov. 2013, pp. 1–4.

[35] M. Mabrouk, S. Rajan, M. Bolic, I. Batkin, H. R. Dajani, and V. Z. Groza, "Detection of human targets behind the wall based on singular value decomposition and skewness variations," in *Proc. IEEE Radar Conf.*, May 2014, pp. 1466–1470.

[36] X. Li, D. Qiao, Y. Li, and H. Dai, "A novel through-wall respiration detection algorithm using UWB radar," in *Proc. 35th Annu. Int. Conf. IEEE Eng. Med. Biol. Soc. (EMBC)*, Jul. 2013, pp. 1013–1016.

[37] M. H. Mostafa, S. Chamaani, and J. Sachs, "Singular spectrum analysis-based algorithm for vitality monitoring using M-sequence UWB sensor," *IEEE Sensors J.*, vol. 20, no. 9, pp. 4787–4802, May 2020.

[38] M. Hinich, "Detecting a hidden periodic signal when its period is unknown," *IEEE Trans. Acoust., Speech, Signal Process.*, vol. ASSP-30, no. 5, pp. 747–750, Oct. 1982.

[39] R. Zetik, S. Crabbe, J. Krajnak, P. Peyerl, J. Sachs, and R. Thoma, "Detection and localization of persons behind obstacles using M-sequence through-the-wall radar," in *Sensors, and Command, Control, Communications, and Intelligence (C3I) Technologies for Homeland Security and Homeland Defense V*, vol. 6201. Bellingham, WA, USA: SPIE, 2006, pp. 145–156.

[40] *ECC Decision (06)04. The Harmonised Use, Exemption From Individual Licencing and Free Circulation of Devices Using Ultra-Wideband (UWB) Technology in Bands Bellow 10.6 GHz*. Accessed: Mar. 24, 2006. [Online]. Available: https://docdb.cept.org/document/397

[41] J. G. Proakis and D. G. Manolakis, *Digital Signal Processing: Principles, Algorithms, and Applications*, 4th ed. Upper Saddle River, NJ, USA: Prentice-Hall, 2006.

[42] J. Rovňáková, *Complete Signal Processing for Through Wall Tracking of Moving Targets*. New York, NY, USA: Academic, Sep. 2010.

[43] D. Urdzik and D. Kocur, "CFAR detectors for through wall tracking of moving targets by M-sequence UWB radar," in *Proc. 20th Int. Conf. Radioelektronika*, Apr. 2010, pp. 1–4.

[44] H. Rohling, "Radar CFAR thresholding in clutter and multiple target situations," *IEEE Trans. Aerosp. Electron. Syst.*, vol. AES-19, no. 4, pp. 608–621, Jul. 1983.

[45] H. Rohling, "Ordered statistic CFAR technique—An overview," in *Proc. 12th Int. Radar Symp. (IRS)*, 2011, pp. 631–638.

[46] G. Minkler and J. Minkler, *CFAR: The Principles of Automatic Radar Detection in Clutter*. Palm Bay, FL, USA: Magellan Book Company, 1990.

[47] J. Rovňáková and D. Kocur, "TOA estimation and data association for through-wall tracking of moving targets," *EURASIP J. Wireless Commun. Netw.*, vol. 2010, no. 1, pp. 1–11, Dec. 2010.

[48] J. Rovňáková and D. Kocur, "Compensation of wall effect for through wall tracking of moving targets," *Radioengineering*, vol. 18, no. 2, pp. 189–195, 2009.

[49] A. Gharamohammadi, F. Behnia, A. Shokouhmand, and G. Shaker, "Robust Wiener filter-based time gating method for detection of shallowly buried objects," *IET Signal Process.*, vol. 15, no. 1, pp. 28–39, Feb. 2021.

[50] A. Gharamohammadi, Y. Norouzi, and H. Aghaeinia, "Optimized UWB signal to shallow buried object imaging," *Prog. Electromagn. Res. Lett.*, vol. 72, pp. 7–10, Jan. 2018.

[51] A. Gharamohammadi, F. Behnia, and R. Amiri, "Imaging based on correlation function for buried objects identification," *IEEE Sensors J.*, vol. 18, no. 18, pp. 7407–7413, Sep. 2018.

[52] M. Svecova, D. Kocur, and R. Zetik, "Object localization using round trip propagation time measurements," in *Proc. 18th Int. Conf. Radioelektronika*, Apr. 2008, pp. 1–4.

[53] S. Blackman, *Multiple-Target Tracking With Radar Applications* (Artech House Radar Library). Norwood, MA, USA: Artech House, 1986.

[54] J. Khan, S. Niar, A. Menhaj, and Y. E. hillali, "Multiple target tracking system design for driver assistance application," in *Proc. Des. Archit. Signal Image Process.*, Brussels, Belgium, Nov. 2008, pp. 126–131.

[55] R. B. Langley, "Dilution of precision," *GPS World*, vol. 10, no. 5, pp. 52–59, 1999.

[56] *ILMSENS GmbH*. Accessed: Mar. 3, 2021. [Online]. Available: http://www.ilmsens.com/

[57] *m:explore M-Sequence System*. Accessed: Mar. 3, 2021. [Online]. Available: https://www.ilmsens.com/products/

[58] *RFspin S.R.O.* Accessed: Mar. 3, 2021. [Online]. Available: https://www.rfspin.cz/en/antennas/measurement-antennas/drh10

Dušan Kocur was born in Košice, Slovakia, in 1961. He received the Ing. (M.Sc.) and C.Sc. (Ph.D.) degrees in radioelectronics from the Faculty of Electrical Engineering and Informatics, Technical University of Košice, in 1985 and 1990, respectively. He is a Full Professor at the Department of Electronics and Multimedia Communications of his Alma Mater. His research interests are radar signal processing, UWB technologies, and their applications.

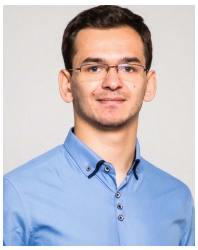

Tamás Porteleky was born in Rimavská Sobota, Slovakia, in 1995. He received the Ing. (M.Sc.) degree in telecommunications from the Faculty of Electrical Engineering and Informatics, Technical University of Košice, in 2019. He currently works at the K-Mlab Organization Unit of Ilmsens GmbH. His research interests are UWB radar signal processing focused on detection, localization and tracking of moving and motionless persons, and estimation of the respiratory rate of motionless persons using UWB sensor networks.

Mária Švecová was born in Svidník, Slovakia, in 1983. She received the M.Sc. degree in mathematics from Pavol Jozef Šafárik University in Košice, Slovakia, and the Ph.D. degree in information electronics from the Technical University of Košice, Slovakia. She is currently with the Department of Mathematics and Theoretical Informatics, Technical University of Košice. Her research interests include UWB radar signal processing with a focus on detection and tracking of moving persons, breathing detection, and localization of motionless persons by UWB sensor systems.

Michal Švingál was born in Lučenec, Slovakia, in 1996. He received the Ing. (M.Sc.) degree in telecommunications from the Faculty of Electrical Engineering and Informatics, Technical University of Košice, in 2019. He is currently working at the K-Mlab Organization Unit of Ilmsens GmbH. His research is focused on UWB sensor networks to be applied for detection, localization, and tracking of moving and motionless persons.

Jana Fortes (Rovňáková) was born in Michalovce, Slovakia, in 1983. She received the M.S. degree in mathematics from Pavol Jozef Šafárik University in Košice, Slovakia, in 2006, and the Ph.D. degree in information electronics from the Technical University of Košice, Slovakia, in 2009. From 2009 to 2014 and since 2020, she has been a Researcher at the Department of Electronics and Multimedia Communications, Technical University of Košice. Her research interests are in UWB radar signal processing applied for detection, localization, and tracking of moving or static persons.